

Atomic Linkage Flexibility Tuned Isotropic Negative, Zero and Positive Thermal Expansion in $MZrF_6$ ($M = Ca, Mn, Fe, Co, Ni$ and Zn)

Lei Hu,[†] Jun Chen,^{†,*} Jiale Xu,[†] Na Wang,[†] Fei Han,[†] Yang Ren,[‡] Zhao Pan,[†] Yangchun Rong,[†] Rongjin Huang,[§] Jinxia Deng,[†] Laifeng Li,[§] Xianran Xing[†]

[†] Department of Physical Chemistry, University of Science and Technology Beijing, Beijing 100083, China

[‡]X-ray Science Division, Argonne National Laboratory, Argonne, Illinois 60439, United States
[§]Key Laboratory of Cryogenics, Technical Institute of Physics and Chemistry, Chinese Academy of Sciences, Beijing 100190, China

1. Experimental section

$MZrF_6$ ($M = \text{Ca, Mn, Fe, Co, Ni}$ and Zn) samples were carefully prepared by a conventional solid state methods. Raw fluoride materials (CaF_2 , MnF_2 , FeF_2 , CoF_2 , NiF_2 , ZnF_2 and ZrF_4 , 99.9%, Alfa Aesar) were used without further processing. Firstly, the powder of MF_2 and ZrF_4 was mixed thoroughly according to 1:1 molar ration, pressed into a pellet, and then loaded into a Cu tube. Subsequently, additional NH_4F powder was filled into the Cu tube in order to protect the final product from oxidization during the reaction process. The Cu tube was sealed completely, which was then sent into a furnace, and heated at $850\text{ }^\circ\text{C}$ for 1 h.

The temperature dependence of synchrotron X-ray diffraction (SXRD) of CaZrF_6 , NiZrF_6 and ZnZrF_6 has been collected at the beamline 11-ID-C of APS, Argonne National Laboratory with high-energy X-ray radiation ($\lambda = 0.117418\text{ \AA}$). The temperature dependence of XRD of all $MZrF_6$ compounds was employed on X-ray diffractometer with Cu $K\alpha$ radiation (PANalytical, PW 3040-X'Pert Pro and BRUKER D8-discover). Powder diffraction structure refinement was performed by the Rietveld method with FULLPROF software based on the cubic symmetry ($Fm\bar{3}m$). Variable temperature dependent synchrotron X-ray total scatterings of pair distribution function (PDF) of

CaZrF₆ and NiZrF₆ were collected at the beamline 11-ID-C with the same wavelength ($\lambda = 0.117418 \text{ \AA}$). G(r) functions were computed using PDFgetX2.¹ Correction, background subtraction, and sample absorption, were also undertaken with PDFgetX2. Structure refinements were carried out using PDFgui.²

In NiZrF₆, Ni \cdots F and Zr \cdots F peaks could only be fitted as one broad peak (M \cdots F) due to the limited XPDF resolution. In CaZrF₆, Ca \cdots F and Zr \cdots F peaks are also treated as one (here is M \cdots F).

All the first-principles calculations were based on density functional theory within the Perdew-Burke-Ernzerhof approximation,³ as implemented in the Vienna ab initio simulation package.⁴ Interactions between ion cores and valence electrons were described by the projector augmented wave method.⁵ Plane waves with a kinetic energy cutoff of 500 eV were used as the basis set. Integration over the Brillouin zone was done with the Monkhorst-Pack scheme⁶ of $8 \times 8 \times 8$ grid points. All of the structures were fully relaxed until the maximum residual ionic force was below 0.01 eV/ \AA . Bader charge analysis was performed for the charge density. Spin-polarized calculations were conducted for NiZrF₆.

2. Results and discussion

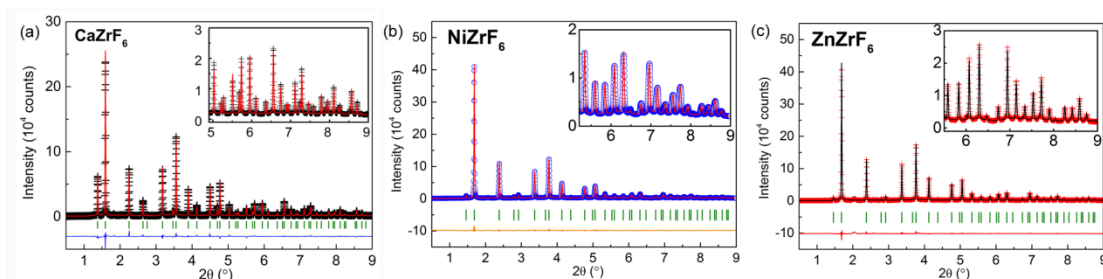


Figure S1. Synchrotron X-ray diffraction patterns for (a) CaZrF_6 (b) ZnZrF_6 and (c) NiZrF_6 . The insets show the high angle regions. Black crosses, blue circles and red crosses are the experimental results. Red and black solid lines indicate the calculated data. Green vertical lines mark the peak positions, and the difference lines are exhibited at the bottom of figure.

The structure refinements have been performed for CaZrF_6 , NiZrF_6 and ZnZrF_6 by means of high-energy synchrotron X-ray diffraction (SXR). As shown in Figure S1, the experimental SXR profile of $M\text{ZrF}_6$ ($M=\text{Ca}$, Ni and Zn) is well modeled with centrosymmetric $Fm\bar{3}m$ space group.

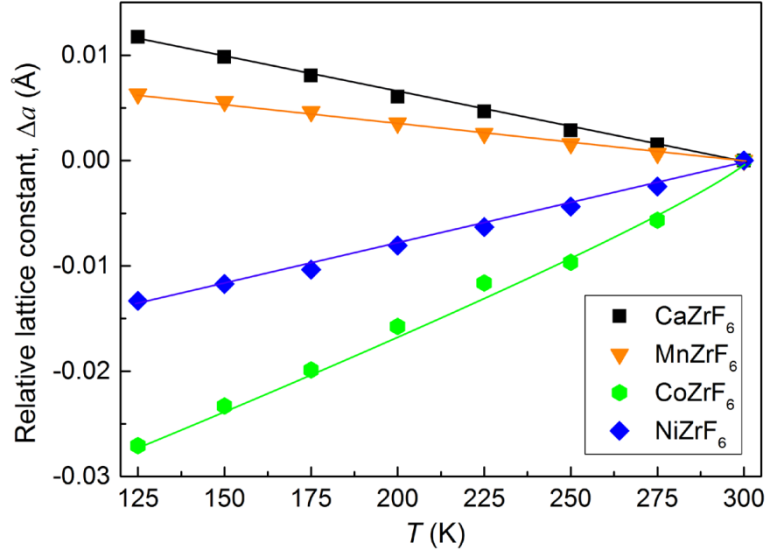


Figure S2. Relative change of lattice constants ($\Delta a = a_T - a_{300\text{K}}$) of $M\text{ZrF}_6$ ($M = \text{Ca}, \text{Mn}, \text{Co}, \text{and Ni}$). CaZrF_6 and MnZrF_6 exhibit NTE with $\alpha_l = -7.91 \times 10^{-6}/\text{K}$ and $-4.40 \times 10^{-6}/\text{K}$, respectively. CoZrF_6 and NiZrF_6 demonstrate PTE with $\alpha_l = +19.39 \times 10^{-6}/\text{K}$ and $+9.62 \times 10^{-6}/\text{K}$, respectively. The CTEs are calculated for the temperature range of 125 K to 300 K.

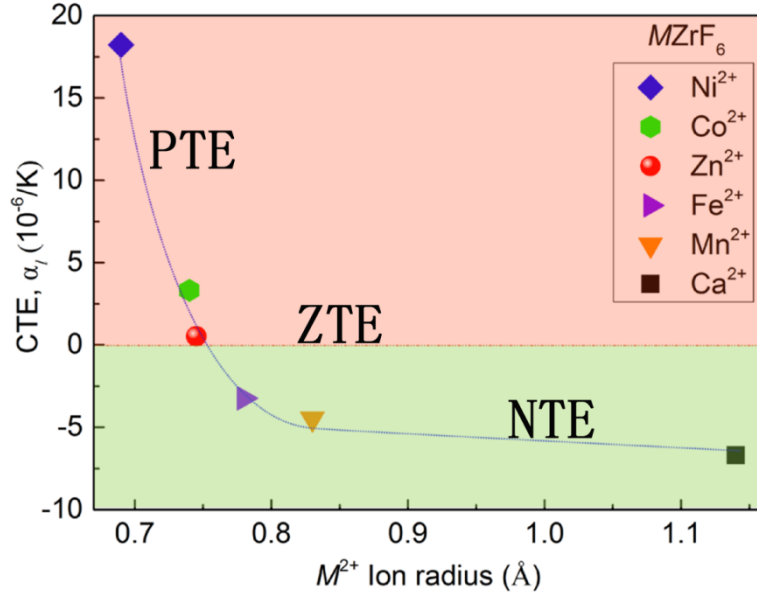


Figure S3. The relationship between the linear CTE, α_l , and the M^{2+} ionic radius for $MZrF_6$ ($M = Ca, Mn, Fe, Co, Ni$ and Zn). The short dot line is a guide to an eye.

The relationship between the linear CTE, α_l , and the ionic radius is presented in Figure S3. It could be seen that the linear CTE, α_l , decreases with increasing M^{2+} ionic radius. As M^{2+} ionic radius increases, the bond strength of M -F presumably decreases and the framework turns to be much more flexible, which facilitates the thermal vibration of fluorine atoms and enhances NTE. Conversely, the smaller M^{2+} ionic radius, such as Zn^{2+} and Ni^{2+} , produces a strongly bonded and commensurately more restricted framework with ultimate ZTE or even considerably PTE properties in $ZnZrF_6$ and $NiZrF_6$, respectively.

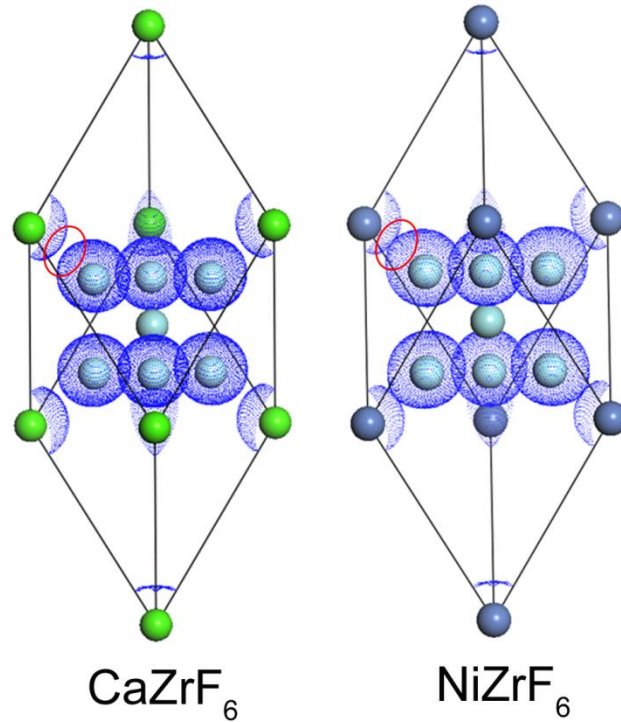


Figure S4. Charge density at the $0.45 e/r_0^3$ isosurface (r_0 : Bohr radius) in CaZrF_6 (left) and NiZrF_6 (right). The interaction section of metal and fluorine atoms is marked by the red ellipses.

As shown in Figure S4, charge density at a specific isodensity surface for the two cases of NTE CaZrF_6 and PTE NiZrF_6 is calculated. As it is marked by the red ellipses, the charge cloud in CaZrF_6 is more localized while more covalent in NiZrF_6 . The electron cloud shifts towards to the atomic interaction section. This physical picture is consistent with the shorter Ni-F distance and higher Ni-F bond strength than that of Ca-F bond, which was revealed by the synchrotron X-ray total scattering analysis.

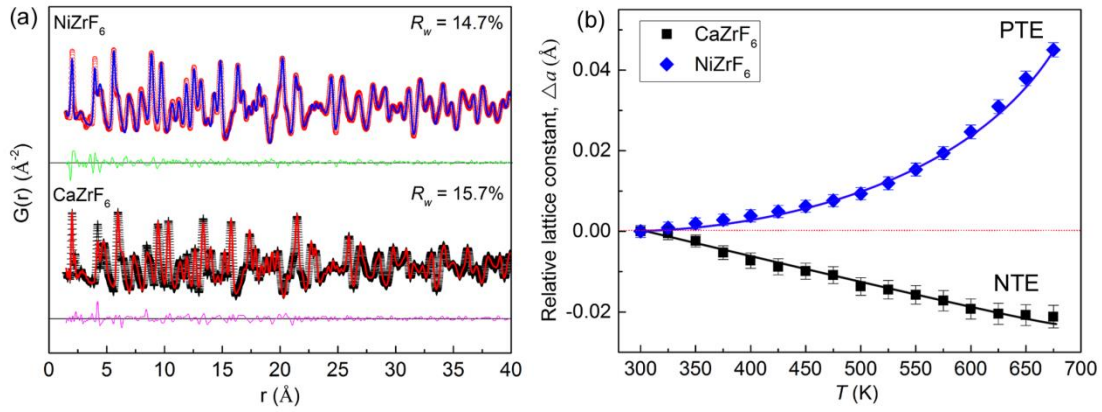


Figure S5. (a) Experimental (black crosses and red circles) and calculated PDFs (red and blue lines) for CaZrF_6 and NiZrF_6 at room temperature. The model is based on the cubic symmetry (space group: $Fm\bar{3}m$). R_w values are agreement factors. (b) Relative change of lattice constant extracted from PDF fits for CaZrF_6 and NiZrF_6 . CaZrF_6 exhibits a strong NTE ($\alpha_l = -6.75 \times 10^{-6}/\text{K}$), while NiZrF_6 shows a considerably PTE ($\alpha_l = +15.33 \times 10^{-6}/\text{K}$). The data of thermal expansion determined from PDF fits have a good agreement with these from SXR.

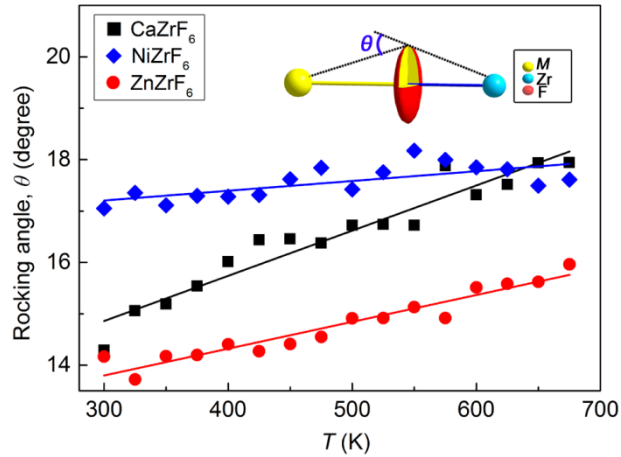


Figure S6. Rocking angle, θ , of $MZrF_6$ ($M = \text{Ca}, \text{Ni}$ and Zn). The inset shows the thermal ellipsoid of fluorine atom (red) which locates between M (yellow) and Zr (cyan) atoms.

The rocking angle is associated closely with the magnitude of fluorine atom thermally displacing away from the ideal position at $(x, 0, 0)$. This angle is attributed to static distortion and dynamic transverse thermal vibration. Temperature dependence of rocking angles could demonstrate the degree of transverse thermal vibration of fluorine atoms. The angle of NTE CaZrF_6 enhances most rapidly with increasing temperature, compared to that of PTE NiZrF_6 and ZTE ZnZrF_6 . The rocking angle in NiZrF_6 is smallest. The prompt raise of the rocking angle with increasing temperature demonstrates a great magnitude of transverse thermal vibration of fluorine atoms, which contributes to the NTE behavior of CaZrF_6 . However, for NiZrF_6 the contribution of transverse thermal vibration is weak, and thus PTE dominates. ZnZrF_6 exhibits isotropic ZTE due to its moderate transverse thermal vibration.

Table S1. Lattice constants of FeZrF₆ and ZnZrF₆ at low temperatures

T (K)	FeZrF ₆		ZnZrF ₆	
	a (Å)	c (Å)	a (Å)	c (Å)
125	5.64107(18)	13.99510(54)	5.57096(14)	13.88477(37)
150	5.65517(18)	13.98745(56)	5.57883(14)	13.87885(36)
175	8.04173(27)		5.59532(13)	13.85885(36)
200	8.05411(27)		5.60112(17)	13.86352(63)
225	8.05613(19)		7.96614(13)	
250	8.05732(18)		7.97415(12)	
275	8.05743(16)		7.97703(10)	
300	8.05778(15)		7.97956(10)	

* FeZrF₆ and ZnZrF₆ transform from cubic symmetry ($Fm\bar{3}m$) to rhombohedral one (space group, $R\bar{3}$) around 150 K and 200 K, respectively.

Table S2. Lattice constants, coefficient of thermal expansion (CTE) and cation radii of cubic $MZrF_6$ ($M = Ca, Mn, Fe, Co, Ni, \text{ and } Zn$)

$MZrF_6$	Lattice constant (\AA)*	CTE($10^{-6}/K$), RT-675 K	Ionic radius, M^{2+} (\AA) ⁷
CaZrF ₆	8.45286(10)	-6.69	1.14
MnZrF ₆	8.17656(8)	-4.47	0.83
FeZrF ₆	8.06987(10)	-3.24	0.78
CoZrF ₆	8.00004(18)	+3.33	0.745
NiZrF ₆	7.92112(9)	+18.23	0.69
ZnZrF ₆	7.98365(7)	+0.52	0.74

* Lattice constants are room temperature values which were calculated from structural refinements of X-ray diffraction patterns.

Table S3. Computed Bader charges (unit in e) of CaZrF_6 and NiZrF_6

Element	Compounds	
	CaZrF_6	NiZrF_6
Ca/Ni	1.69	1.57
Zr	3.59	3.53
F	-0.88	-0.85

In order to investigate the bonding characteristics, the Bader charge analysis of two representative compounds, CaZrF_6 (strong NTE) and NiZrF_6 (considerable PTE), is presented in Table S3. It is observed that the positive charges of metal atoms (*M* and Zr) decrease along with the increase of the negative charges of fluorine atom from CaZrF_6 to NiZrF_6 . This significant change in the Bader charge of metal and fluorine atoms of the two compounds shows that the Ni/Zr-F interaction is much less polarized compared with that of CaZrF_6 . And the covalent component of the chemical bonds in NiZrF_6 is fair larger than that of the Ca/Zr-F interaction in CaZrF_6 .

Table S4. Isotropic thermal expansion properties in the representative NTE compounds with open framework structures.

Compounds	Space group	Linear CTE, α_l ($10^{-6}/\text{K}$)	T range (K)	Reference
$MPt(\text{CN})_6$ ($M = \text{Mn, Fe, Co, Ni, Zn, Cd}$)	$Fm\bar{3}m$	-10.02 – -1.02	100 – 400	8
$\text{LnCo}(\text{CN})_6^\dagger$ ($\text{Ln} = \text{La, Sm, Ho, Lu, Y}$)	$P6_3/mmc$	-14.62 – -9.05	100 – 420	9
$M_3[\text{Co}(\text{CN})_6] \cdot n\text{H}_2\text{O}$ ($M = \text{Mn, Fe, Co, Ni, Cu, Zn}$)	$F\bar{4}3m$	-39.7 – -19.6	123– 298	10
$M_3[\text{Fe}(\text{CN})_6] \cdot n\text{H}_2\text{O}$ ($M = \text{Mn, Fe, Co, Ni, Cu, Zn}$)	$F\bar{4}3m$ or $Fm\bar{3}m$	-39.6 – +47.8	123–298	10
$M(\text{CN})_2$ ($M = \text{Zn and Cd}$)	$Pn\bar{3}m$	-16.9 (Zn) -20.4 (Cd)	25 – 375 (Zn), 150–375 (Cd)	11
$M_2\text{O}$ ($M = \text{Cu, Ag}$)	$Pn\bar{3}m$	-2.4 (Cu) -10.4 (Ag)	9 – 240 (Cu) 10 – 500 (Ag)	12
$\text{Zn}_{1-x}\text{Sn}_x\text{Mo}_2\text{O}_8$	$Pa\bar{3}$	-5.9 – +7.9	12 – 500	13
$(\text{Sc}_{1-x}\text{M}_x)\text{F}_3$ ($M = \text{Ga, Fe, Al}$)	$Pm\bar{3}m$	-3.3 – +3.3	300 – 900	14
$M\text{ZrF}_6$ ($M = \text{Ca, Mn, Fe, Co, Ni, Zn}$)	$Fm\bar{3}m$	-6.69 – +18.23	300 – 673	This study

\dagger $\text{LnCo}(\text{CN})_6$ is near isotropic negative thermal expansion material.

3. References

- (1) Qiu, X.; Thompson, J. W.; Billinge, S. J. *J. Appl. Crystall.* **2004**, *37*, 678.
- (2) Farrow, C.; Juhas, P.; Liu, J.; Bryndin, D.; Božin, E.; Bloch, J.; Proffen, T.; Billinge, S. J. *Physics: Condensed Matt.* **2007**, *19*, 335219.
- (3) Perdew, J. P.; Burke, K.; Ernzerhof, M. *Phys. Rev. Lett.* **1996**, *77*, 3865.
- (4) Kresse, G.; Furthmüller, J. *Comput. Mater. Sci.* **1996**, *6*, 15.
- (5) Blöchl, P. E. *Phys. Rev. B* **1994**, *50*, 17953.
- (6) Monkhorst, H. J.; Pack, J. D. *Phys. Rev. B* **1976**, *13*, 5188.
- (7) Shannon, R. T. *Acta Crystallogr. Sect. A: Cryst. Phys., Diffr., Theor. Gen. Crystallogr.* **1976**, *32*, 751.
- (8) Chapman, K. W.; Chupas, P. J.; Kepert, C. J. *J. Am. Chem. Soc.* **2006**, *128*, 7009.
- (9) Duyker, S. G.; Peterson, V. K.; Kearley, G. J.; Ramirez - Cuesta, A. J.; Kepert, C. J. *Angew. Chem. Int. Ed.* **2013**, *52*, 5266.
- (10) Adak, S.; Daemen, L. L.; Hartl, M.; Williams, D.; Summerhill, J.; Nakotte, H. *J. Solid State Chem.* **2011**, *184*, 2854.
- (11) Goodwin, A. L.; Kepert, C. J. *Phys. Rev. B* **2005**, *71*, 140301.
- (12) Tiano, W.; Dapiaggi, M.; Artioli, G. *J. Appl. Crystallogr.* **2003**, *36*, 1461.

(13) Tallentire, S. E.; Child, F.; Fall, I.; Vellazarb, L.; Evans, I. R.; Tucker, M. G.; Keen, D. A.; Wilson, C.; Evans, J. S. *J. Am. Chem. Soc.* **2013**, *135*, 12849.

(14) Hu, L.; Chen, J.; Fan, L.; Ren, Y.; Rong, Y.; Pan, Z.; Deng, J.; Yu, R.; Xing, X. R. *J. Am. Chem. Soc.* **2014**, *136*, 13566.